Prabha Materials Science Letters
Vol. 5, No. 2, 378-402, 2026
https://doi.org/10.33889/PMSL.2026.5.2.021

Simulating the Heat Transfer in a Receiver and Thermal Energy Storage for a Concentrated Solar Power (CSP) Plant

Alistair Bascom
Department of Electrical Engineering,
University of Guyana, Georgetown, Region 4 (Demerara-Mahaica), Guyana.
E-mail: alistair.bascom@gmail.com

(Received on November 5, 2025; Revised on January 10, 2026 & April 6, 2026; Accepted on April 17, 2026)

Abstract
Renewable energy fosters the green energy transition to keep the global temperature increase below 1.5 ℃. Concentrated solar power (CSP) with thermal energy storage (TES) can reduce emissions, leading to energy independence. A CSP plant in Guyana would lead to economic development and clean energy. CSP technology has not been deployed in Guyana, so this study highlights CSP and TES as a solution for Guyana. The study utilised MATLAB to create the Guyana CSP Potential App as a computational tool. This is to computationally model the CSP and TES system for a Guyana location, which is pertinent before investment. The rationale of a just transition was explored as a criterion for recommending Corriverton over Georgetown as the final location for the CSP plant, although the Georgetown CSP plant would have marginally better energy output than the Corriverton CSP plant. Direct normal irradiance (DNI) and air temperature for Georgetown and Corriverton were obtained from RETScreen. The heliostat was $100{,}000\ \mathrm{m^2}$. Solar salt was the heat transfer material chosen. The Corriverton DNI ($\mathrm{kWh/m^2}$) has a maximum of $5.68\ \mathrm{kWh/m^2}$ in September, and Corriverton Air Temperature (℃) having a maximum of 27.8 ℃ in October. The Corriverton CSP Energy Output (MWh) has a maximum of 3.5150×10^3 MWh in September, the Corriverton CSP System Efficiency (%) has a maximum of 21.3063 % in January, the Corriverton Thermal Energy Storage (MWh) achieves its highest capacity as 3.1049×10^3 MWh in September, and while Corriverton Thermal Energy Loss (MWh) has a maximum loss of 1.9643×10^3MWh in September.

Keywords- Concentrated solar power, Energy output, MATLAB, Thermal energy storage, System efficiency.

1. Introduction

1.1 Model of CSP with TES

Concentrated solar power (CSP) uses mirrors that focus sunlight onto a receiver. This results in a high temperature that can drive a turbine and generate electricity. CSP is unlike photovoltaic panels, which can convert sunlight directly into electricity. CSPS behaves similarly to a conventional thermal power plant. It is well-suited for integrating heat engines into thermal industrial processes. CSP can generate dispatchable power that is available in regions of high solar concentration. However, electricity demands often peak at night, rising from about sunset. CSP technology represents a small amount of the global solar capacity, but it is expanding, particularly in countries with high solar irradiance and large-scale renewable infrastructure.

Thermal energy storage (TES) can make CSP technology competitive by storing heat in molten salt or solar salt, so plants can produce electricity when the sun is not shining. Hence, providing a reliable on-demand renewable power. TES systems can use either a two-tank direct, two-tank indirect or a single-tank thermocline design. Each design must balance cost, efficiency and fluid compatibility issues. In the typical two-tank system, heat is collected during the day and stored at high temperature in the tank. Later, the high temperature is used to generate steam for electricity production at night or during cloudy periods. The dispatchability of CSP with a TES plant allows it to smooth the variability of renewable energy and supports grid stability. CSP with TES compete with PV-plus-battery systems for the solar energy market, but the deployment of both technologies will foster the clean energy transition.

Modelling the CSP tower, which has a TES, involves multiple subsystems such as the solar field or heliostat field, the receiver on the tower, the thermal energy storage (TES) system, and lastly the power block, which can be the Rankine cycle. There is an intermittency in solar energy that needs to be resolved (Pan et al., 2023).

The solar field can be concentrated, and the heliostat field focuses solar radiation onto a receiver. The optical power collected is given by:

$$Q_{solar} = DNI \cdot A_{field} \cdot \eta_{optical} \tag{1}$$

In Equation (1), where, DNI is direct normal irradiance $[W/m^2]$, A_{field} is the total mirror area $[m^2]$ and $\eta_{optical}$ is the optical efficiency.

$$\text{Optical efficiency} = \text{cosine loss} \times \text{shading/blocking} \times \text{reflectivity} \times \text{intercept factor} \times \text{etc.} \tag{2}$$

Equation (2) shows the formula for the optical efficiency. The optical efficiency in this research was not derived but used as an estimated value.

At the receiver, in this case, heat absorption on the tower, thermal power absorbed:

$$Q_{receiver} = Q_{solar} \cdot \eta_{receiver} \tag{3}$$

In Equation (3), where, $\eta_{receiver}$ is the receiver efficiency, which includes the thermal losses due to conduction, convection and radiation.

$$T_r = \frac{E_{receiver}}{m_{salt} \cdot c_p} + T_{amb} \tag{4}$$

In Equation (4), where, $E_{receiver}$ is the energy at the receiver, T_r is the temperature of the salt in the receiver, m_{salt} is the mass of the salt (solar salt) in the receiver, c_p is the specific heat capacity of the solar salt and T_{amb} is the temperature of the surrounding air.

$$\rho_{salt} = \frac{m_{salt}}{V_{salt}} \tag{5}$$

In Equation (5), where ρ_{salt} is the density of solar salt and V_{salt} is the volume of solar salt in the receiver and the tubing.

$$1 \text{ Wh} = 3{,}600 \text{ J} \tag{6}$$

Equation (6) shows the conversion used to convert between Joules and Watt-hours for this research.
Next, the thermal power losses of the receiver are given by:

$$Q_{loss} = Q_{cond} + Q_{conv} + Q_{rad} \tag{7}$$

Equation (7) show the conductive, convective and radiative losses summing to the thermal loss.

where, conductive loss is:

$$Q_{cond} = \frac{k \cdot A_c \cdot (T_r - T_{amb})}{L} \tag{8}$$

In Equation (8), where, k is the thermal conductivity of the receiver wall or insulation $[W/m \cdot K]$, A_c is the conduction area or cross-sectional area for heat flow, and L is the thickness of the receiver wall or insulation.

Convective loss is:

$$Q_{conv} = h \cdot A_r \cdot (T_r - T_{amb}) \tag{9}$$

And the Radiative loss is:

$$Q_{rad} = \epsilon \cdot \sigma \cdot A_r \cdot \left(T_r^4 - T_{amb}^4\right) \tag{10}$$

In Equations (9) and (10), where, h is the convective heat transfer coefficient $[W/m^2 K]$, ϵ is the emissivity, σ is the Stefan-Boltzmann constant $\sigma = 5.67 \times 10^{-8}\ W/m^2 K^4$, A_r is the receiver area, T_r is the receiver temperature and T_{amb} is the ambient temperature. CSP plants use mirrors to reflect light to the receiver and TES to store energy; the energy generated by this method can be optimised (Pinello et al., 2023).

For the thermal energy storage (TES), a common TES medium is molten salt. The energy stored is given by:

$$E_{storage} = m_{salt} \cdot c_p \cdot (T_{hot} - T_{cold}) \tag{11}$$

In Equation (11), where m_{salt} is the mass of the molten salt, c_p is the specific heat of the salt and T_{hot} and T_{cold} are the inlet and outlet temperatures, respectively. However, the adoption of HTFs has been limited due to viscosity challenges; mixtures can be adopted to reduce viscosity (Kwasi-Effah et al., 2024).

The charging relationship during the day is:

$$Q_{charge} = \dot{m} \cdot c_p \cdot (T_{hot} - T_{cold}) \tag{12}$$

In Equation (12), where, Q_{charge} is the power stored when charging and $\dot{m}$ is the mass flow rate.

The discharge to the power block is given by:

$$Q_{discharge} = \dot{m}_{dis} \cdot c_p \cdot (T_{hot} - T_{cold}) \tag{13}$$

In Equation (13), where, $Q_{discharge}$ is the discharge power and $\dot{m}_{dis}$ is the discharge flow rate.

where, $\dot{m}$ is the mass flow rate, $\dot{m}_{dis}$ is the discharge flow rate, and c_p is the specific heat capacity of the salt. Solid particles can be used as an HTF and in TES as a material for next-generation applications (Nie et al., 2022). Compressed air can be used as an HTF in a small-scale application; this novel solar innovation can be modelled for a solar plant configuration (Grena et al., 2024).

Examining the power block, for example, the Rankine cycle, some key assumptions must be made. For the thermal power to the cycle is:

$$Q_{in} = Q_{discharge} \tag{14}$$

Equation (14) show input of the Rankine cycle, which is the energy absorbed by the receiver minus the losses.

And the electric power output is:

$$W_{ele} = Q_{input} \cdot \eta_{cycle} \tag{15}$$

In Equation (15), where, η_{cycle} the efficiency of the Rankine cycle is typically between 35 – 45%.

The overall system efficiency can be found as follows:

$$\eta_{system} = \frac{W_{ele}}{DNI \cdot A_{field}} = \eta_{optical} \cdot \eta_{receiver} \cdot \eta_{storage} \cdot \eta_{cycle} \tag{16}$$

Equation (16) show the derivation of system efficiency used in this research.

CSP technologies may find applications in solar thermal desalination plants (Cekirge et al., 2020a). CSP plants can be designed to utilise the Brayton cycle for the third-generation CSP and Rankine cycle for TES to electricity generation (Cekirge et al., 2020b).

Table 1 shows the constants used to compute the thermal power absorbed.

Table 1. The constants used in computing thermal power absorbed by the heliostat area.

Total Helical Field Area	$100{,}000\ \mathrm{m^2}$
Optical Efficiency	70 %
Absorber Efficiency of the Receiver	85 %

Table 2 shows the constants used to compute the power loss, net power and receiver temperature.

Table 2. The constants used in computing power loss, net power and receiver temperature.

Emissivity of Silicon Oxide Coating	0.1
Stefan-Boltzmann Constant	$5.67 \times 10^{-8} \times 10^{-6}\ \frac{\mathrm{MW}}{\mathrm{m^2K^4}}$
Heat Transfer Coefficient	$10 \times 10^{-6}\ \frac{\mathrm{MW}}{\mathrm{m^2K}}$
Density of Solar Salt	$1{,}800\ \frac{\mathrm{kg}}{\mathrm{m^3}}$
Volume of Solar Salt	$700\ \mathrm{m^3}$
Specific Heat Capacity of Solar Salt	$1{,}500\ \frac{\mathrm{J}}{\mathrm{kgK}}$

Table 3 shows the constants used to compute the energy output, thermal energy loss and system efficiency.

Table 3. The constants used in computing energy output, thermal energy loss and system efficiency.

Rankine Cycle Efficiency	43 %
Total Helical Field Area	$100{,}000\ \mathrm{m^2}$

Table 4 shows the constants used to compute the thermal energy stored in the tank.

Table 4. Constants used in computing thermal energy stored in the tank.

Mass of Solar Salt	$18 \times 10^6\ \mathrm{kg}$
Specific Heat Capacity of Solar Salt	$1{,}500\ \frac{\mathrm{J}}{\mathrm{kgK}}$
Cold Tank Temperature	530 K

1.2 Objectives

Concentrated solar power (CSP) has a small global installed capacity as a form of solar energy conversion. Solar energy is abundant and comes from the sun. This energy can be utilised for generating electricity. Photovoltaics is the popular method for converting solar energy to electricity for the utility grid. CSP offers an alternative form of conversion for solar energy. As the main energy source in the solar system is the sun, research on alternative conversion approaches is necessary, and even more so for a growing branch of solar energy conversion, such as CSP, to make it deployable. Hence, this investigation studies the CSP technology by creating a MATLAB app to assess the thermal losses, electrical energy production and system efficiency for a Georgetown location, Demerara-Mahaica (Region 4) and a Corriverton location, East Berbice-Corentyne (Region 6), where the construction of a CSP plant will be recommended to be built at one of the locations in Guyana.

Thermal energy storage (TES) technology can improve CSP deployment, as it would provide a means of storing energy in non-peak hours and making it available at night when demand is high. TES would allow energy for the grid during cloudy days, thus increasing grid stability. The TES will be computed, and the TES system capacity at each study location will be determined.

The novelty of this research is creating a model for a CSP with TES and conducting the assessment for two locations in Guyana. Also, attempting to model the CSP with the TES system by creating a working MATLAB app for assessment, contributes to understanding CSP with TES systems by attempting to understand the computations behind the energy conversion. The idea of a just transition was explored to rationalise the final recommendation of the CSP with the TES system for the development of Guyana, so that the renewable energy transition fairly develops the lives of everyone in the country.

2. Concentrated Solar Power (CSP)

2.1 Generation

The deployment of renewable energy technologies requires polygeneration and hybridisation of the grid to increase grid reliability. Simulations can be used to model renewable systems before deployment. Software such as RETScreen and MATLAB are indispensable for computations related to renewable energy systems (Bascom, 2025). CSP plants are used for electricity generation, but up until now, the technology has not been affordable for developing countries. To improve CSP technology, ceramic balls of clay and industrial waste can be developed into sensible heat storage. Models predicting the behaviour of the ceramic oil and vegetable oil for thermal energy storage (TES) systems were developed. The results show that the possibility of discharge is in 9 hours and has an efficiency of 90%. The development of ceramic balls could be considered an innovation and a cost-effective measure for CSP and TES technology (Bagré et al., 2023). Solar power is an effective means of generating electricity and promoting a carbon-neutral grid. Heat transfer materials (HTMs) are important for CSP Systems and their accessory TES devices. HTMs are divided into categories based on their physical properties, which are either liquid, gaseous or solid. The main HTMs for TES devices in CSP systems are liquid metals, water, molten salts, heat transfer oils and nanofluids (Wang et al., 2023).

Solar energy has the potential to reduce dependence on fossil fuels via CSP technologies. CSP plants with TES can produce electrical energy that is based on the thermodynamic power cycle. Solar collectors, reflectors, thermal fluids, turbines and receivers are the main components of CSP plants and heat transfer is involved at every stage. The thermal fluid characteristics remain stable across a wide range of operational conditions. The heat capacity, vapour pressure, and volume expansion of thermal fluids should not differ significantly at different temperatures, across various stages. Variations can cause failure if not designed for. CSP Technologies are generally higher in cost compared to electricity generated from gas power plants.

Efforts are being made to make it sustainable and inexpensive. The main impediment to CSP technology is the intermediate nature of the sun. Modern CSP technology is integrated with TES units to smooth power production (Alnaimat & Rashid, 2019).

A dual-loop solar field, with solar salt as the transfer fluid in a parabolic or linear Fresnel solar collector, was studied. Supercritical carbon dioxide (s-CO_2) in a Brayton power cycle was the system applied. Oil has advantages as a transfer fluid, seeing that it is widely deployed across numerous power plants. A plus is also that there is less corrosion when using oil than molten salts. The maximum temperature threshold with oil is about 400℃ with plant efficiencies of 37% due to the Carnot principle. Solar salt is a mixture of 60% Sodium Nitrate ($NaNO_3$) and 40% Potassium Nitrate (KNO_3). The maximum operating temperature of this is 550℃, but it has a freezing temperature of 220℃. This pipe will require electrical heating to prevent the solidification of the salt (Coco-Enríquez et al., 2017). An approach towards TES of surplus renewable energy is to introduce hybrid thermochemical or sensible heat storage concepts, which implement porous structures made of redox metal oxides and are capable of reduction or oxidation, upon heating or cooling of direct air. This would accompany an endothermic or exothermic heat effect, which demonstrates fully that the reversible dimension of the reaction can give a heat effect (Agrafiotis et al., 2023).

2.2 Software Approximation

The thermal analysis of CSP plants can be conducted considering either parabolic trough collectors, linear Fresnel collectors and direct steam generation. The analysis focused on the environmental conditions of the location in Chile, in the study. The thermal performance can be an indicator; likewise, the solar field aperture and power block range are indicators of the system. Transient simulations were considered an open-access model was developed (Starke et al., 2016). Heat transfer fluid (HTF) can be evaluated for its performance in CSP systems. The Noor I CSP plant in Morocco was modelled using the System Advisor Model (SAM). Simulations were conducted to assess the thermal and economic performance of silicon-based HTF. The objective was to identify the fluid to enhance the efficiency and cost-effectiveness of the plant (Yahya et al., 2024).

Solar central receiver configuration is a development in solar technology and promises to be useful to CSP. It provides an alternative to the working fluid by using solar-heated air for the CSP working fluid. Auxiliary burners are required to extend the operation of the off-sunshine hours without TES. The configuration was adopted by the 1.5 MW Julich CSP power plant in Germany. Air was used as the heat transfer fluid in the solar tower to produce steam via the Rankine cycle. A simulation of the Julich plant having TES or hybrid CSP, which uses air as a working fluid, was performed. Considerations were the yearly operations, and the determination of the exergy and exergoeconomic cost was derived (Catalano et al., 2016).

A model and simulation were conducted on the CSP plant in Ber'Alganam of the Azzawia-Libya area. The thermal analysis of this solar power plant was conducted to identify the characteristics of the present monthly power curve for the measured solar irradiance, given the meteorological data of Ber'Alganam. Mathematical models of the solar plant were based on the energy balance of each component, and a simulation was created in MATLAB. The simulation tool was used to simulate the solar plants, and the desired plots from the results were displayed. Among the CSP technologies for a parabolic trough collector and a 30MW CSP plant was proposed for the hourly performance and productivity of the year. The study also offered a TES and a backup boiler (Abuashe et al., 2020).

2.3 CSP Plants

The world is transitioning towards stable and sustainable energy consumption. This transition is evident in the energy sector, as modern renewable technologies, such as photovoltaics and wind farms, are expanding their global reach. The Rankine cycle steam turbine can be used to convert solar thermal energy into electricity with a 42% to 45% efficiency. The next generation of solar concentrated solar power technologies will require fluids and thermal energy storage to lower the cost and achieve temperatures as high as 565℃ (Khan et al., 2022a). CSP is the conversion of the sun's thermal energy from incoming radiation using mirrors or optical elements to focus the sunlight on a receiver containing a liquid such as water or molten salt. The fluid is heated to generate steam, which in turn rotates a steam turbine and produces electricity. The CSP plant may contain thermal energy storage (TES). The direct solar radiation (DNI) represents 90% of the sunlight on a sunny day. On a cloudy day, CSP plants are not effective. CSP plants work well when located in the sunbelt around the equator, particularly in the Middle East, Africa and India. Areas with DNI greater than $2{,}800\ \mathrm{kW/m^2}$ per year, are good areas for CSP plants (Shukir, 2022).

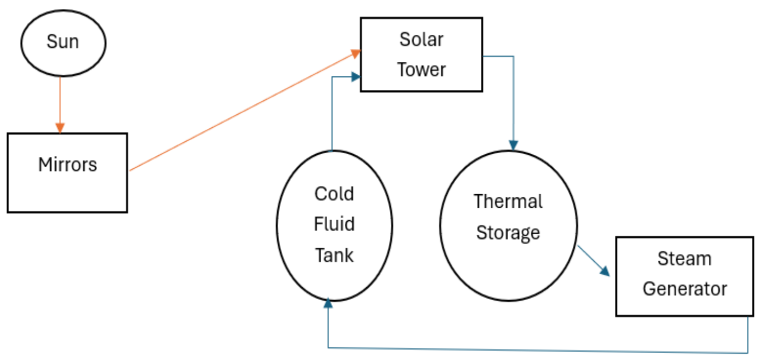

Figure 1. Block diagram of CSP plant (Shukir, 2022).

Figure 1 shows the CSP concept for this research. It uses direct solar irradiation to heat a working fluid and generate electricity. A typical CSP is a combination of a solar concentrator, a heat transfer fluid and a power generation block. The CSP technology is a renewable energy source via sunlight. Although sunlight is an intermittent source by nature. Sunlight can be converted into thermal energy and stored in TES. Incorporating TES ensure a steady supply of energy on cloudy days or nights. The TES can utilise sensible, latent, or thermochemical energy, with combinations used for TES. Nanotechnology can also enhance the heat transfer, having superior thermal properties over conventional fluids (Jawhar et al., 2020).

In the preservation of our agricultural products for export, drying has become an outstanding tool. Solar parabolic trough collectors are being used to dry agricultural products to effectively remove moisture. Heat transfer fluids HTFs flow through the receiver tube and absorb solar radiation. To reduce heat loss, the pipe is insulated. Solar dryers are being designed to be concentrated-type solar dryers with dryer chambers. The dryer has a thermal efficiency of about 30% and shows considerable moisture removal for a given ginger sample taken experimentally. The temperature difference in the dryer chamber showed an increase of 11 ℃, proving more effective than open-air drying (Bori et al., 2024). Solar energy is expected to become the primary source of electricity production in the future. CSP systems are highly dependent on the efficiency of reflectors and receivers. CSP technologies are designed to use a working medium and TES to deal with the intermittent electrical power generated from solar energy. Hybrid systems or cogeneration are possible alternatives. Receivers with a smaller aperture can operate under higher solar concentration ratios to produce high temperatures when in focus. The construction of materials for receivers and heat transfer media is vital for the extraction of solar energy, either via mirror fields or parabolic collectors. Phase change materials (PCM) can have numerous applications in energy collection and in storage systems (Onu & Mbohwa, 2019).

2.4 Power Generation from CSP

Concentrated solar power (CSP) technologies are advancing and are becoming competitive as they improve performance. Thermal energy storage (TES) is a major contributor to the breakthrough. Small scales, TES and CSP are suitable for distributed generation, for example, a 10 MW plant using the Rankine Cycle, Organic Rankine Cycle, or Open Gas Cycle power block to optimise performance (Abaza et al., 2020). Global trends have led to the development of CSP technologies, including Linear Fresnel Reflectors. Solar radiation is concentrated via a flat, slightly curved reflector onto a receiver tube through which water flows. Steam is directly generated here as a heat transfer fluid used to store heat. The performance of this system is essential to improve the levelized cost of electricity (LCOE) and the capacity factor of the system (Tahir et al., 2024).

The central receiver-based system for CSP technology has evolved significantly to allow grid-connected plants and aims to be competitive in the energy transition (Hernández et al., 2025). Solar central receiver configuration is a promising application of CSP plants. CSP can use solar-heated air as a working fluid in a Brayton thermal cycle and the heat transfer fluid for the Rankine thermal cycle, as an alternative to the regular working fluid. This reduces the operational maintenance of the system and provides a higher degree of flexibility for the power section (Toro et al., 2016).

2.5 Thermal Energy Storage

Particle-based thermal energy storage (TES) can be used with a concentrated solar power (CSP) plant. The key concept is the fluidised bed heat exchanger, which can be used as a particle-based storage system and operates at 91% efficiency (Reyes-Belmonte et al., 2018). CSP technologies are promising in that they can generate power for the coming decades. However, because solar energy availability is sometimes unstable, certain factors affect the integration of CSP technologies. Hence, TES are required for CSP plants. Heat transfer fluids for TES may require sensible energy storage that can suffer from low energy density. Phase change materials (PCM) have motivated the deployment of latent heat TES (Khan et al., 2022b).

A model of a CSP plant with two tanks for direct storage was developed using the gPROMS platform. A eutectic mixture of sodium nitrate salt and potassium was used as the heat transfer fluid as well as the storage medium. Ten years' worth of solar radiation for Isfahan city was used in the study. The storage system had been designed to feed a boiler for 15 hours in the absence of sunlight, and the instantaneous effects were computed, given solar radiation on the CSP plant (Goortani & Heidari, 2017). Energy from CSP plants can be optimised via storage systems. Power plants are increasingly required to store energy capacity to stabilise the energy balance. Superheated steam is fed to a turbine for efficient energy conversion. This team can be controlled by a steam actuator right before entering the turbine. The TES cycle has a capacity based on the material used for storage. A stable absorption can enhance thermal stability in the CSP power plant application, and materials for storage should be studied for optimising the overall plant (Atmaja & Pikra, 2013).

TES offers advantages to extend the operation of power dispatch for a CSP. Dual-media TES are cost-effective and reduce the need for heat transfer fluids, which are usually made from expensive materials. One strategy is to start with a cold storage tank, which is referred to as a cold start, and another is to start with a fully charged storage tank, which is a hot tank. These methods were investigated concerning their effect on electrical energy production over the same period. An enthalpy model for the energy storage and temperature variation was made, and each HTF was applied to both sensible heat storage systems and latent heat storage systems. The analysis was conducted on the plant, but for a 60 MWe and found that the cold start was beneficial to both sensible and latent heat systems compared to the hot start (Xu et al., 2015). CSPS rely on TES technologies to extend operation via heat storage for efficient energy systems. Bauxite powder has been known for its ability and high temperature stability and has now emerged as an alternative to conventional materials for CSP deployment. Particle shape, packaging and heat transfer characteristics of non-spherical particles were studied. The impact of sphericity was compared by contrasting spherical particles and non-spherical particles, ellipsoids, and cylindroids, exploring the effects of these shapes of particles on the retention of energy. It was observed that the cylindroids were better at energy retention. This insight can optimise TES media in CSP plant systems (Boribayeva et al., 2024).

3. Data and Method

3.1 MATLAB CSP App

This research will consist of a literature study on Concentrated Solar Power (CSP) plants and Thermal Energy Storage (TES) systems. The researcher will create an app using MATLAB to simulate a CSP plant with a TES system. The CSP plant will be a tower version upon which the receiver will sit. Reflecting mirrors will reflect the sunlight onto the receiver. A molten salt will be heated up, and this will transfer to the power block and TES. The power block will be based on the Rankine cycle. The idea to conduct this study on CSP technology was brainstormed with Copilot. Gemini and ChatGPT were also used in brainstorming potential formulas for use and providing ideas for potential coding. The researcher reviewed the ideas and formulations that the three different AIs gave and built the code in MATLAB tailored to the specific objectives of the research, and the available information and data obtained for the study. The researcher had a discussion with Copilot on simulation topics for renewable energy research. Copilot suggested the simulation of a CSP system as one of its suggestions. The researcher took the idea and prompted both ChatGPT and Gemini on the topic. Eventually, the form of this research theme was reached. The researcher prompted Copilot, ChatGPT and Gemini for formulas specific to the research goals for the simulation. The AI tools responded with different formulas. The researcher kept refining the prompts until the pool of formulas in the introduction was obtained. The researcher would prompt the AI tools for coding approaches; however, these were not used as output. The researcher manually typed the code after reviewing the examples and methods given by Copilot, ChatGPT and Gemini. During the typing of the MATLAB code, the researcher would prompt the AI tools for addition formulas, specific information on CSP and TES technologies that would help in coding, and would check the MATLAB website for discussions on specific debugging issues. The AI tools were also instrumental in debugging. The graphs were plotted in both the MATLAB App and an M-file, and the M-file graphs were presented in the research.

3.2 Simulation Heat Transfer in Receiver

The primary objective of the study is to simulate a CSP plant which has a TES system. To do this, the researcher needs to simulate the solar field or heliostat field. The DNI and area of the solar field would be required to compute energy from the sun. The DNI will be obtained from RETScreen for 2 locations in Guyana: 1 in Region 4, Demerara-Mahaica and 1 in Region 6, East Berbice-Corentyne. Next, the receiver on the tower must be simulated. Heat would be absorbed by the receiver on the tower. The receiver efficiency would determine how much of the solar energy is converted to energy transmitted to the receiver. The receiver efficiency would be dependent on the losses due to conduction, convection and radiation. The thermal losses need to be accounted for if a realistic receiver energy is going to be estimated.

3.3 Simulation Thermal Energy Storage

Examining the TES system, the total energy stored by the system needs to be computed. This can be done by using the mass of the molten salt, the salt's specific heat capacity and the hot inlet and cold outlet temperatures. Daytime charging energy needs to be modelled using the mass flow rate of the salt during the day. During hours of discharge, the mass flow rate of the salt during discharge needs to be noted, and the discharging energy transferred to the power block.

3.4 Simulation Power Block

The input of the power block will be the discharge of the TES system. However, not all the input power that goes to the power block will be converted into electrical energy for output to the grid. The efficiency of the Rankine cycle will determine the conversion to electrical energy. The last computation will be the determination of the system efficiency. For all the individual sections of coding and conceptualisation, Copilot, ChatGPT & Gemini played an important role in brainstorming ideas and presenting an iteration of the computation methods to achieve the simulation of a CSP plant with a TES system. Copilot was the AI tool that suggested simulating a CSP plant during the researcher's discussion with the tool on research avenues. ChatGPT and Gemini, the researcher asked for formulas that would realise the simulation. The responses were reviewed, and the researcher continued to prompt both AI tools with increasingly specific prompts, almost iteratively, after each review, until suitable formulas were obtained. The researcher also used the pool of formulas to prompt ChatGPT and Gemini, mainly for coding approaches; however, the AI tools made some mistakes and employed approaches that the researcher would not have employed. However, these approaches were reviewed, and the researcher wrote the code for the app according to the researcher's personal preferences when coding and built the app according to what seemed suitable, considering the suggestions of the AI tools. Copilot, ChatGPT and Gemini were instrumental during debugging.

4. Results

4.1 Sensitivity Analysis

The objective of first conducting the sensitivity analysis was two-fold. Firstly, the sensitivity analysis played a crucial part in troubleshooting the software. The app was coded with careful consideration, but still produced high results that were considered erroneous. The researcher troubleshooted the code, checking what each modification did to the result. The researcher employed troubleshooting techniques by displaying certain results in the MATLAB command window. The researcher also prompted ChatGPT and Copilot throughout the troubleshooting process to gain an understanding of the specifications of real-life CSP plants. Secondly, after the sensitivity analysis was completed, the researcher used the final sensitivity analysis result to reflect a calibration for the results of the app. This will give an idea to the reader whether the app produces realistic results.

Table 5. The inputs of sensitivity analysis used in the Guyana CSP potential app.

Trial Number	Month	CSP Plant DNI (kWh/m^2)	Air Temperature (℃)
1	January	0.001	25
2	February	0.010	25
3	March	0.100	25
4	April	1.000	25
5	May	2.000	25
6	June	3.000	25
7	July	4.000	25
8	August	5.000	25
9	September	6.000	25

Table 5 shows the input for the sensitivity analysis. Note that the sensitivity analysis does not represent realistic data for any month. The air temperature was held constant at 25℃ so that DNI variations can be tested to see the responses of the software. The researcher does not use this data to inform about real-world data, but based on the sensitivity analysis results, the researcher was better able to debug the code for the Guyana CSP Potential App to produce more realistic results. Hence, it was data out together for the debugging process to improve the code. The Direct Normal Irradiance (DNI) was varied, while the air temperature was held constant. The air temperature would have affected the computation of the losses, but varying the air temperature was not considered a critical factor, as the air temperature in Guyana, a tropical country, varies between $25 - 27$℃. In the calculation of the losses, that variation in air temperature or ambient temperature is quite negligible. Trial 9 reflected a DNI larger than any of the DNI data obtained from RETScreen.

Table 6. The output of sensitivity analysis for Guyana CSP potential app, energy and efficiency.

Trial number	Month	CSP plant energy output (MWh)	CSP plant system efficiency (%)	CSP plant thermal energy storage (MWh)	CSP plant thermal energy Loss (MWh)
1	January	0.6968	22.4764	0	0.2241
2	February	6.2931	22.4755	0	2.0248
3	March	69.6452	22.4662	0	22.4845
4	April	670.4532	22.3484	0	225.8065
5	May	1.3736×10^3	22.1551	0	494.5379
6	June	1.9694×10^3	21.8821	811.1250	775.0282
7	July	2.6678×10^3	21.5148	1.6611×10^3	1.1737×10^3
8	August	3.2610×10^3	21.0388	2.5111×10^3	1.6387×10^3
9	September	3.6791×10^3	20.4396	3.3611×10^3	2.1539×10^3

Table 6 shows the output for the sensitivity analysis conducted on the Guyana CSP Potential App. The 4 key results obtained from the sensitivity analysis were the CSP Plant Energy Output (MWh), CSP Plant System Efficiency (%), CSP Plant Thermal Energy Storage (MWh) and CSP Plant Thermal Energy Loss (MWh). For trials $5 - 9$, the energy output was between $1{,}000 - 3{,}000$ MWh for a month. The months from January to September were used in the simulation, simply because the app was built to take inputs over a period of a year. The thermal energy storage only stores energy where the T_{hot}, the temperature of the tank is greater than 530 ℃. If T_{hot} falls below this preset value, energy can no longer be stored. The energy discharge of the TES was not simulated, just the maximum energy stored given the DNI. The thermal losses were due to convective losses, conductive losses and radiative losses. It was clearly seen that thermal losses increased with increasing DNI as $T_{receiver}$ the temperature of the receiver would increase with greater incident radiation reflected by the heliostat area. Note that thermal losses are almost as high as the electricity generated. These results do not compute the other losses in energy which occur at every stage, but from the system efficiency, roughly $(78 - 80)\%$ of the energy reflected by the heliostat is lost, with the energy generated comparable to the thermal losses alone.

Table 7. The output of sensitivity analysis for Guyana CSP potential app, temperature.

Trial number	Month	Ambient temperature (K)	Receiver temperature (K)
1	January	298.15	298.2633
2	February	298.15	299.2833
3	March	298.15	309.4833
4	April	298.15	411.4833
5	May	298.15	524.8167
6	June	298.15	638.1500
7	July	298.15	751.4833
8	August	298.15	864.8167
9	September	298.15	978.1500

Table 7 shows the Ambient Temperature (K), which is the Air Temperature that was inputted and the Receiver Temperature (K). The receiver temperature was derived dynamically based on the energy reflected by the heliostat area. The highest receiver temperature reached was 978.1500 K.

4.2 Gyana CSP Potential App, Simulation

The tables below show the input and results of the simulation of Guyana CSP Potential App.

Table 8. The inputs used in Guyana CSP potential app.

Months name	Month number	Georgetown DNI (kWh/m^2)	Corriverton DNI (kWh/m^2)	Georgetown air temperature (℃)	Corriverton air temperature (℃)
January	1	4.39	4.46	26.1	25.6
February	2	5.14	4.83	26.4	25.7
March	3	5.00	5.09	26.7	26.1
April	4	4.94	4.98	27.0	26.6
May	5	4.92	4.67	26.8	26.2
June	6	4.56	4.66	26.5	25.6
July	7	5.50	5.04	26.6	25.5
August	8	5.78	5.38	27.0	26.1
September	9	5.61	5.68	27.5	27.1
October	10	5.44	5.44	27.6	27.8
November	11	5.14	4.96	27.2	27.5
December	12	4.78	4.50	26.4	26.4

Table 8 shows the DNI of both Georgetown and Corriverton. The Georgetown location achieves higher irradiance for some months. The DNI data are comparatively similar, and CSP location can be well-suited if placed at either Corriverton or Georgetown. Georgetown is in Demerara-Mahaica, Region 4, while Corriverton is in East Berbice-Corentyne, Region 6. Guyana does not currently utilise CSP technology. This study also highlights the potential of Guyana as a CSP generator. The air temperatures are slightly greater in Georgetown than in Corriverton. The DNI data was sourced from ground stations data and obtained from RETScreen, while the air temperature was obtained from RETScreen, this time via NASA data.

Table 9. The primary outputs for Guyana CSP potential app.

Months name	Month number	Georgetown CSP energy output (MWh)	Corriverton CSP energy output (MWh)	Georgetown CSP system efficiency (%)	Corriverton CSP system efficiency (%)
January	1	2.9036×10^3	2.9458×10^3	21.3359	21.3063
February	2	3.0154×10^3	2.8567×10^3	20.9522	21.1231
March	3	3.2591×10^3	3.3107×10^3	21.0264	20.9820
April	4	3.1205×10^3	3.1431×10^3	21.0563	21.0379
May	5	3.2133×10^3	3.0692×10^3	21.0683	21.2007
June	6	2.9074×10^3	2.9651×10^3	21.2526	21.2097
July	7	3.5366×10^3	3.2832×10^3	20.7426	21.0136
August	8	3.6850×10^3	3.4720×10^3	20.5657	20.8178
September	9	3.4785×10^3	3.5150×10^3	20.6682	20.6281
October	10	3.5027×10^3	3.5025×10^3	20.7704	20.7688
November	11	3.2299×10^3	3.1311×10^3	20.9462	21.0420
December	12	3.1331×10^3	2.9689×10^3	21.1439	21.2821

Table 9 shows the energy output and the system efficiency for both potential plants. The maximum energy produced by the Georgetown CSP plant is 3.6850×10^3 MWh in August, while the Corriverton CSP plant would output 3.5150×10^3 MWh in September. The table also displays the system efficiency of the

respective systems. The highest system efficiency was associated with January for both CSP plants. Georgetown CSP had a system efficiency of 21.3359 %, while Corriverton CSP had a system efficiency of 21.3063 %. The lower the DNI in a month, the better the system efficiencies.

Table 10. The secondary output for Guyana CSP potential app.

Months name	Month number	Georgetown thermal energy storage (MWh)	Corriverton thermal energy storage (MWh)	Georgetown thermal energy loss (MWh)	Corriverton thermal energy loss (MWh)
January	1	2.009×10^3	2.0566×10^3	1.3448×10^3	1.3757×10^3
February	2	2.6406×10^3	2.3719×10^3	1.5506×10^3	1.4033×10^3
March	3	2.5239×10^3	2.5959×10^3	1.6432×10^3	1.6891×10^3
April	4	2.4751×10^3	2.5061×10^3	1.5608×10^3	1.5799×10^3
May	5	2.4566×10^3	2.2396×10^3	1.6021×10^3	1.4761×10^3
June	6	2.1484×10^3	2.2266×10^3	1.3783×10^3	1.4225×10^3
July	7	2.9481×10^3	2.5489×10^3	1.9201×10^3	1.6610×10^3
August	8	3.1891×10^3	2.8424×10^3	2.0915×10^3	1.8490×10^3
September	9	3.0484×10^3	3.1049×10^3	1.9244×10^3	1.9643×10^3
October	10	2.9046×10^3	2.9061×10^3	1.8882×10^3	1.8888×10^3
November	11	2.6466×10^3	2.4959×10^3	1.6635×10^3	1.5721×10^3
December	12	2.3346×10^3	2.0966×10^3	1.5304×10^3	1.3959×10^3

Table 10 shows the thermal energy storage for both the Georgetown and Corriverton CSP plants. August has the highest storage of 3.1891×10^3 MWh, for Georgetown, and September has the highest for energy storage for the Corriverton CSP plant at 3.1049×10^3 MWh. In terms of thermal energy loss, Georgetown CSP would have 2.0915×10^3 MWh in August, while Corriverton CSP would have 1.9643×10^3 MWh of losses in September. These reflect the maximum for the year.

Table 11. The tertiary output for Guyana CSP potential app.

Months name	Month number	Georgetown ambient temperature (K)	Corriverton ambient temperature (K)	Georgetown receiver temperature (K)	Corriverton receiver temperature (K)
January	1	299.2500	298.7500	796.7833	804.2167
February	2	299.5500	298.8500	882.0833	846.2500
March	3	299.8500	299.2500	866.5167	876.1167
April	4	300.1500	299.7500	860.0167	864.1500
May	5	299.9500	299.3500	857.5500	828.6167
June	6	299.6500	298.7500	816.4500	826.8833
July	7	299.7500	298.6500	923.0833	869.8500
August	8	300.1500	299.2500	955.2167	908.9833
September	9	300.6500	300.2500	936.4500	943.9833
October	10	300.7500	300.9500	917.2833	917.4833
November	11	300.3500	300.6500	882.8833	862.7833
December	12	299.5500	299.5500	841.2833	809.5500

Table 11 shows the ambient temperatures (K) for both Georgetown and Corriverton sites and the receiver temperatures (K) for the two locations. The ambient temperature is needed to calculate receiver temperature and thermal losses. The receiver temperature was lowest in January for both Georgetown, with 796.7833 K and for Corriverton, with 804.2167 K. For the Georgetown CSP plant, the highest receiver temperature was 955.2167 K in August, while the Corriverton CSP plant had the highest receiver temperature, it was 943.9833 K in September.

4.3 Guyana CSP Potential App, Graphs

The data for the graphs are from the Guyana CSP Potential App.

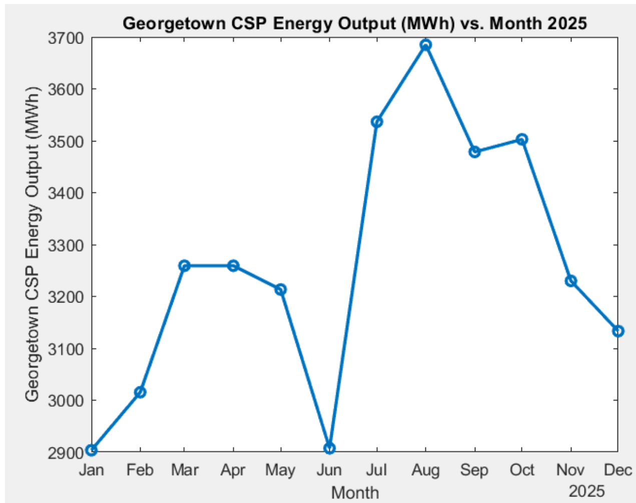

Figure 2. Prospective Georgetown CSP plant energy output (MWh).

Figure 2 shows the prospective energy output (MWh) of a potential Georgetown CSP Plant. The graph describes the energy that would be produced over the course of a single year. March is depicted as an initial peak in energy output, followed by a decrease in April. The lowest energy would be produced in January and June. September has the peak in expected energy production and gradually decreases after that.

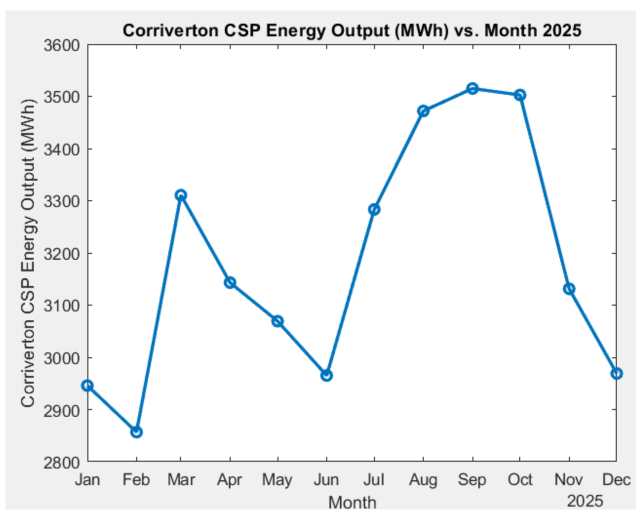

Figure 3. Prospective Corriverton CSP plant energy output (MWh).

Figure 3 shows the energy output (MWh) for a prospective Corriverton CSP Plant. From the graph, the lowest month for energy production is February. March indicates an initial peak as seen. June is the next low point in energy production, but it is higher than January and February. August, September and

November are generally the better months in the Corriverton area for utilising CSP energy production. According to the graphs, more energy is produced in the Georgetown area than in the Corriverton area during the peak months of production. Observing the earlier months, particularly January and February, when energy production is lower, the georgetown CSP Plant would produce more energy than the Corriverton CSP Plant for the lower productive months; June is a marked exception. However, between the two plants, the Georgetown CSP plant would be a better choice to construct based on energy production.

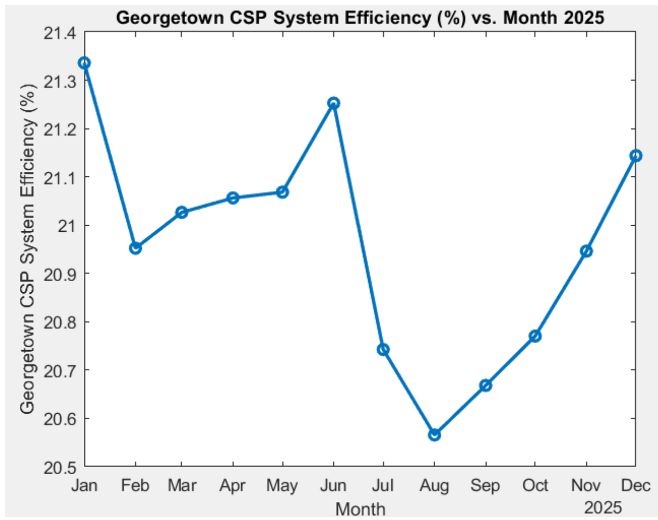

Figure 4. Prospective Georgetown CSP plant system efficiency (%).

Figure 4 shows the system efficiency (%) for the prospective Georgetown CSP Plant that was simulated in this study. Higher efficiencies are associated with months of lower energy production. This is the result of the lower thermal losses during those months. August had the lowest system efficiency, while January had the highest.

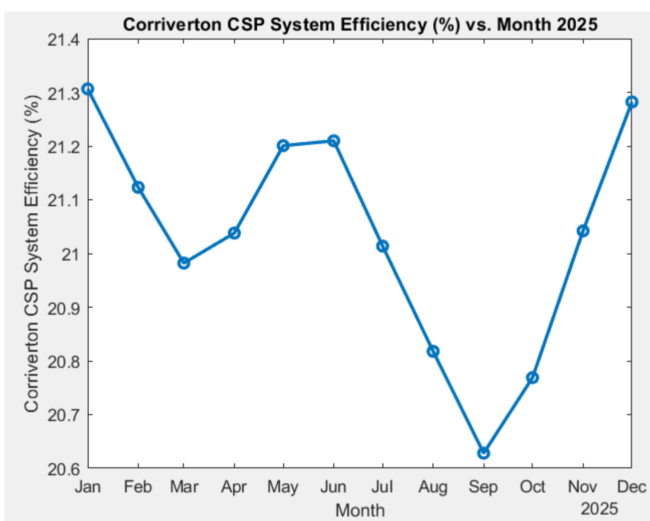

Figure 5. Prospective Corriverton CSP plant system efficiency (%).

Figure 5 shows the system efficiency (%) for the prospective Corriverton CSP plant. The system efficiency is generally low during periods of high energy generation and is high during periods of low energy generation. The reason for this is that thermal energy losses increase with higher temperatures of the absorber. Heat is lost from the absorber via conductive, radiative and convective losses. There is also a conversion efficiency at various stages in the CSP plant, which results in the 20.5 – 21.5 % system efficiency for both plants. The Corriverton CSP plant would have marginally better system efficiency as it handles a lower energy output (MWh) and operates at a lower receiver temperature. September has the lowest system efficiency, and January has the highest.

5. Discussion

5.1 Flow Chart of Model

The flow chart below shows the model used to create the Guyana CSP Potential App.

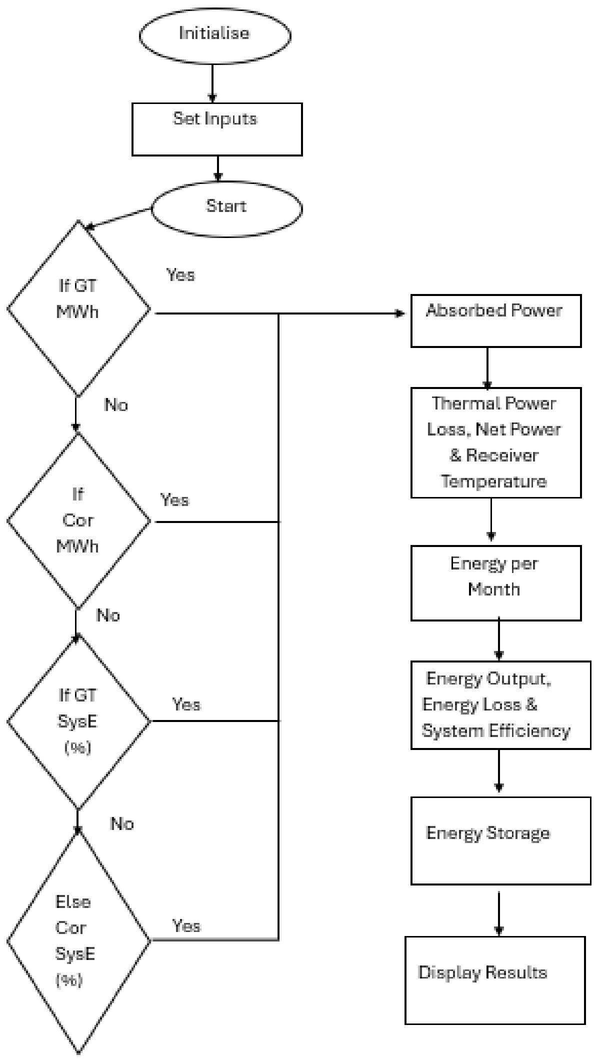

Figure 6. Guyana CSP potential app.

Figure 6 shows the flow chart of the Guyana CSP Potential App. When the app is opened, the first step is to click the Initialise push button. This prepares the tables for input by setting the cells initially. After the initialisation, the input values are set. The radio button that sets the if condition must be set. The Start push button is clicked, and the If condition is recorded.

The first computation is the calculation of the absorbed power. The next function call results in the computation of the thermal power losses. The net power is calculated, as well as the receiver temperature. The third function calculates the energy produced per month, before it is converted to electricity. As the energy transition is undertaken, it becomes necessary to meet the increasing energy demand, and CSP can help fulfil that demand (Khan et al., 2022b).

The fourth function gives the energy output computed using the Rankine cycle, the losses were converted to energy and the system efficiency computed. The fifth function represented the storage capacity of the thermal energy storage tank. Lastly, all the necessary results were displayed. The radio button condition was used to plot the appropriate graph on the axes.

5.2 Simulation of CSP and TES

To conduct the calculation for the concentrated solar power (CSP) and the thermal energy storage (TES) computation, key functions were created to conduct the simulation. Here, the researcher will discuss each of the functions and the constants used. In the first function, where the thermal power absorbed was computed, key constants were $100{,}000\ \mathrm{m}^2$ which was chosen as the helical field area, the optical efficiency was 70% and the absorber efficiency of the receiver was 85%.

For the second function, where the power loss, net power and receiver temperature were computed. The emissivity of the Silicon Oxide ($\mathrm{SiO_2}$) the coating had lower emissivity and was 0.1. The Stefan-Boltzmann constant is $5.67 \times \frac{10^{-8}}{10^{6}} \frac{\mathrm{MW}}{\mathrm{m^2\,K^4}}$, while the convective heat transfer coefficient was $10 \times 10^{-6} \frac{\mathrm{MW}}{\mathrm{m^2\,K^4}}$. The density of the solar salt is $1{,}800\ kg/m^3$ and the volume of the receiver for the molten salt was $700\ \mathrm{m}^3$. The specific heat capacity of the solar salt used was $1{,}500 \frac{\mathrm{J}}{\mathrm{kgK}}$ and to convert between the Degrees Celsius and Kelvin scales, the formula $\mathrm{T_{ambient}} = \theta_{\mathrm{AirTemp}} \times \left(\frac{\mathrm{K}}{{}^{\circ}\mathrm{C}}\right) + 273.15\ \mathrm{K}$. The third function had the conversion of MJ to MWh. The fourth function had the Rankine efficiency of 43%, While for the fifth function, the mass of the molten salt or solar salt in the TES tank was $18 \times 10^{6}\,\mathrm{kg}$ and the solar salt should not fall below $530\ \mathrm{K}$ for the system, even though the melting point of the solar salt is $496\ \mathrm{K}$. The composition of solar salt for TES is a mixture of 60% Sodium Nitrate ($\mathrm{NaNO_3}$) and 40% Potassium Nitrate ($\mathrm{KNO_3}$) by weight. As the global energy landscape is transforming, there is a real need for energy storage that can be accessible and deployable on a large scale (Yahya et al., 2024).

5.3 Comparison of the Results

The sensitivity analysis helped the researcher troubleshoot the app. Appropriate corrections were made to make the work realistic. The Guyana CSP Potential App has been refined to enable dynamic computation of the receiver temperature. The main outputs are the monthly CSP Plant Energy Output (MWh), monthly CSP Plant System Efficiency (%), the storage capacity of the CSP Plant Thermal Energy Storage (MWh) and the monthly CSP Plant Thermal Energy Loss (MWh). Note that system efficiency reflects the percentage of the total incident energy that is converted into electricity. The CSP plant where the computation was done was in Georgetown and Corriverton. MATLAB was used to model a CSP plant in the Ber’Alganam area (Azzawia-Libya) (Abuashe et al., 2020).

The Inputs were the Georgetown DNI ($\mathrm{kWh/m^2}$) with maximum as $5.78\ \mathrm{kWh/m^2}$ in August, Corriverton DNI ($\mathrm{kWh/m^2}$) having a maximum of $5.68\ \mathrm{kWh/m^2}$ in September, Georgetown Air Temperature (℃) with a maximum of 27.6 ℃, in October and Corriverton Air Temperature (℃) having a maximum of 27.8 ℃ in October. Thus, Georgetown will provide better DNI for the CSP plant. Highlighting the maximums for the results, the Georgetown CSP Energy Output (MWh) had a maximum of 3.6850×10^3 MWh in August, while Corriverton CSP Energy Output (MWh) maxed at 3.5150×10^3 MWh in September, thus Georgetown is marginally better than Corriverton from the viewpoint of energy output as electricity. In terms of system efficiency, the Georgetown CSP System Efficiency (%) was a maximum of $21.3359\ \%$ in January, while the Corriverton CSP System Efficiency (%) was maxed at $21.3063\ \%$ in January. The Corriverton CSP plant did perform marginally better than the Georgetown CSP plant for many of the other months. However, greater system efficiencies are associated with lower DNI.

Looking at the thermal energy storage capacity for each month, the Georgetown Thermal Energy Storage (MWh) maxed its capacity in August with 3.1891×10^3 MWh, while the Corriverton Thermal Energy Storage (MWh) achieved its highest capacity as 3.1049×10^3 MWh in September. Again, this indicates that it is marginally better to build the CSP plant close to Georgetown. In terms of thermal energy loss, the Georgetown Thermal Energy Loss (MWh) had a maximum loss of 2.0915×10^3 MWh in August, while Corriverton Thermal Energy Loss (MWh) had a maximum loss of 1.9643×10^3 MWh in September. From the losses, it is marginally better to build the CSP plant in Corriverton. However, these reflect thermal losses only. A CSP plant with TES can be used rather than a natural gas facility (Abuashe et al., 2020).

5.4 Site Selection and Benefits

Before making the selection between the two communities, it is better to examine the benefits of building the CSP plant. There are energy and environmental advantages of a CSP plant, for example, a reliable power supply can be achieved by using the sunlight to generate heat that can be stored or converted to electricity. Thermal storage would be necessary because of given the imminent sunsets that would occur and cloudy days are likely. CSP plants significantly lower emissions of greenhouse gases compared to the use of fossil fuels as a source of energy. This results in cleaner air and a healthier environment. CSP plants are designed to use less water than traditional thermal power plants. In this case, the CSP design uses solar salt as a heat exchange material and can use sustainable water for the plant. The concern with global emissions and the environment naturally trends towards a renewable energy solution (Pinello et al., 2023).

Economic development and workforce development result from jobs for the CSP plant and thermal energy storage (TES) system. Jobs will be created particularly in the construction phase, such as engineering, procurement and construction roles. The operation and maintenance phase of the plant requires long-term roles for the upkeep of the plant. Not to mention the development of skills of the local community, which would require training in welding, electrical work and mechanical maintenance, which are all transferable skills. There are also transitional opportunities for workers in the fossil sector to shift to a renewable energy role. This can be achieved through certification via programs that can help with the transition. CSP is promising, and the use of TES can be integrated into the CSP system (Pinello et al., 2023).

The community will also be impacted by the infrastructure project, in that local investment can be made into the plant and bring upgrades to the community in terms of roads, utility services and benefits. The electricity for the community provides energy independence by gaining control of renewable energy resources that are resilient in place of fossil fuels, which are imported. This will lead to grid stability. The long-term cost savings are significant, though the initial investment is high for CSP systems. CSP systems offer low maintenance costs and provide long-term economic returns. Some countries are even considering beam-down plants that direct energy in space to a precise location on Earth, where the plant is located (Pinello et al., 2023).

The ideal location for a CSP plant requires high Direct Normal Irradiance (DNI), making it ideal for sunny, rural areas with available land. Inclusive development requires the right policies to support the CSP plant. For example, the just and inclusive energy transition needs to be in underserved regions to have an impact on the lives of the wider population. Considering this and the aim of having a just transition, it is optimal to build the CSP plant with TES in Corriverton, East Berbice-Corentyne, Region 6.

6. Conclusion

The Guyana CSP Potential App was created for this research. The app is initialised and then takes in direct normal irradiance (DNI) and air temperature for Georgetown and Corriverton sites. The radio button decides what plot will be made on the axes in the app, and the click of the Start push button runs the computation. The simulation is of a concentrated solar power (CSP) plan with thermal energy storage (TES) capability. The helical field area is $100{,}000\ \mathrm{m}^2$. Solar salt is the heat transfer material used. The simulation was done for both the Georgetown and Corriverton sites; even though the Georgetown site had marginally greater energy output, it was deemed necessary for a just transition to renewable energy to have the CSP plant recommended to be built in Corriverton. The Corriverton DNI ($\mathrm{kWh/m^2}$) has a maximum of $5.68\ \mathrm{kWh/m^2}$ in September, and Corriverton Air Temperature (℃) has a maximum of 27.8 ℃ in October. The Corriverton CSP Energy Output (MW) is a maximum of 3.5150×10^3 MWh in September, the Corriverton CSP System Efficiency (%) is a maximum of 21.3063 % in January, the Corriverton Thermal Energy Storage (MWh) achieves its highest capacity as 3.1049×10^3 MWh in September, and while Corriverton Thermal Energy Loss (MWh) has a maximum loss of 1.9643×10^3 MWh in September.

The CSP plant would supply the community and grid with electricity and TES. The CSP would lower carbon emissions from the current use of fossil fuels. There will be economic development as well as job creation in both the construction phase and operational phase of the CSP plant. The community will be upskilled through training that will be transferable to other employment. Workers in the traditional energy sector can take up new roles in renewable energy and become certified for the energy transition. Investment is going to upgrade the community as a benefit, and the grid will gain greater independence from oil suppliers by utilising renewable energy. Although CSP requires a high initial investment, it has low maintenance costs, thus providing a long-term economic return. CSP is optimal for sunny, rural areas with a lot of available land, with the aim of a just and inclusive transition. It was optimal to recommend the building of a CSP and TES in Corriverton, East Berbice-Corentyne, Region 6.

Conflicts of Interest

The author of this paper had no conflict of interest in the writing of this paper.

Acknowledgments

Thanks to Copilot, ChatGPT and Gemini for the role of the AI tools in this research. Thanks to Dr Jomo Gill for his discussions on the writing of this paper. Anne Bascom and Carlene Bascom for their encouragement. In memory of Carlton Bascom Jr.

AI Disclosure

During the preparation of this work, the author used generative AI in order to improve the language of the article. After using this tool/service, the author reviewed and edited the content as needed and takes full responsibility for the content of the publication.

Appendix

App layout of the Guyana CSP Potential App.

Figure 7 shows the Guyana CSP Potential app. When the app is opened, the user must click Initialise. The Initialise button sets the initial value of the editable tables. There are two tables. Table: Direct Normal Irradiance (Input) is an editable table that takes in Direct Normal Irradiance (DNI) (kWh/m^2) for georgetown and Corriverton obtained on RETScreen. The table also takes in the Air Temperature in (℃) for Georgetown and Corriverton. The radio button is then selected as Corriverton CSP (MWh), Georgetown CSP (MWh) or Corriverton CSP (%) or Georgetown CSP (%). The radio button control determines which graph is displayed on the axes. The options are energy output or system efficiency for the two locations. However, setting the radio button does not result in the graph being plotted. The Start button must be clicked for the computation to be performed, which will then display the axes for the radio button selected. The click of the Start button also results in calculated Energy Output (MWh), Energy Efficiency (%), Thermal Energy Storage (MWh) and Thermal Energy Loss (MWh) for both the prospective Georgetown CSP and Corriverton CSP Plants.

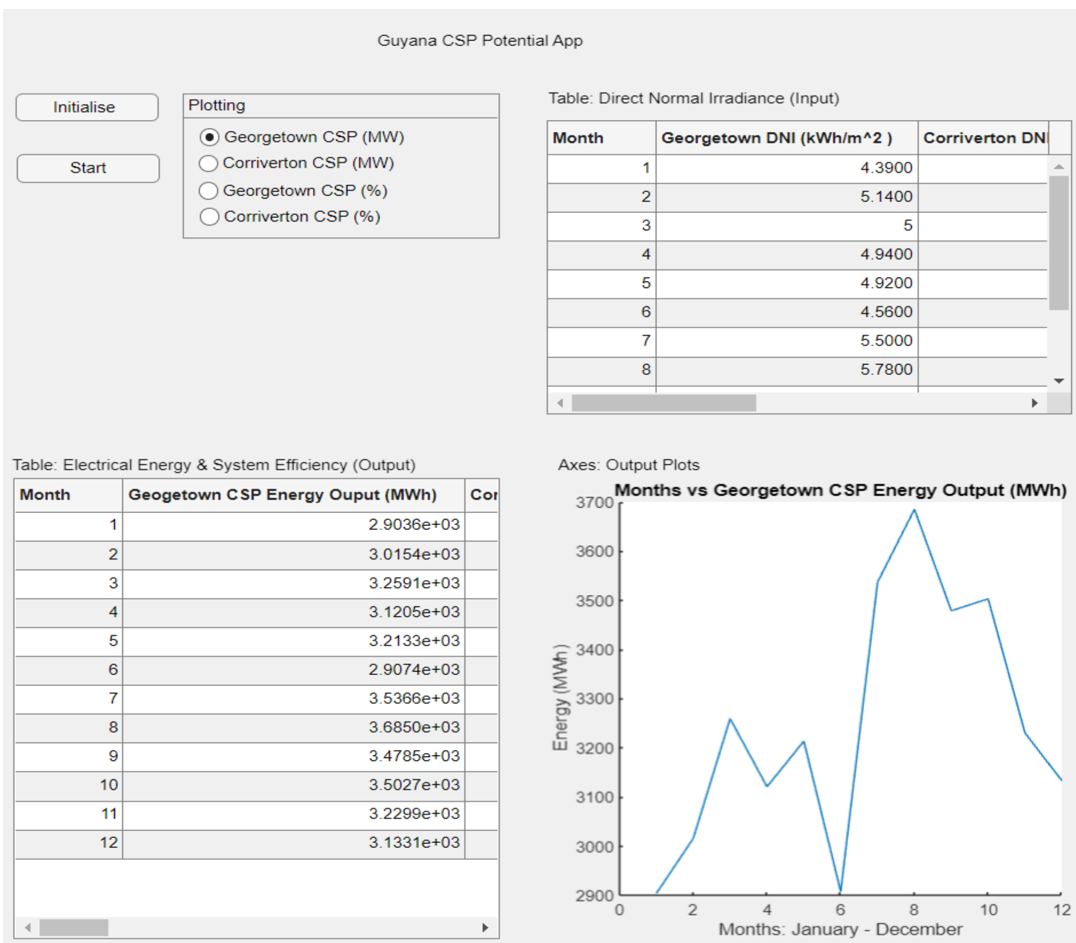

Figure 7. Screenshot of Guyana CSP potential app.

Code 1 shows the computation of absorbed thermal power for the input DNI.

Code 1: Code for computing thermal power absorbed from heliostat area.

```
function Qabs = optpwcollected(app, DNImonthly) %optical power absorbed
    Afield = 100000; % the total helical field area (m^2)
    etaoptical = 0.7; % the optical effficiency
    etareceiver = 0.85; % the absorber efficiency of the receiver

    for n = 1:12
    Qsolar(n) = DNImonthly(n)*Afield; % the incident power (MW)
    Qabs(n) = Qsolar(n)*etaoptical*etareceiver; %absorbed thermal power

    end
end
```

Code 2 shows the code used to compute the receiver temperature, power loss, and net power.

Code 2: Code for computing power loss, net power and receiver temperature.

```
function [Qnet, Qloss, Tr] = thermalLoss(app, Qabs, AirTemp) %Determine Qnet after loasses
    epsilon = 0.1; %emissivity Silicon Oxide coating to lower emissivity.
    sigma = 5.67*10^(-8)/(10^(6)); %Stefan-Boltzmann constant (MW/m^2K^4)
    h = 10/(10^(6)); %Convective heat transfer coefficient (MW/m^2K)
    mreceiver = 1800*700; %  density (kg/m^3) * volume (m^3) = mass of receiver large molten salt (kg)
    cpsalt = 1500;  %specific heat capacity of salt [J/kg.K] Solar Salt
    for n = 1:12
    Tamb(n) = AirTemp(n) + 273.15; %Convertion fro Degrees Celcius to Kelvin
    Tr(n) = (Qabs(n)*1000000*12*3600)/(mreceiver*cpsalt) + Tamb(n);  %approximate receiver surface temperature

    end

    k = 0.15/(10^(6)); % the conductivity of insulation (MW/mK)
    L = 0.1; %Insulation thickness (m)
    Acond = 100; %Conducting area (m^2)
    Areceiver = 500; %Receiver surface area (m^2)

    for n = 1:12
    Qconv(n) = h*Areceiver*(Tr(n)-Tamb(n)); %Convective loss (MW)
    Qrad(n) = epsilon*sigma*Areceiver*((Tr(n)^4)-(Tamb(n)^4)); %radiative loss (MW)
    Qcond(n) = k*Acond*(Tr(n)-Tamb(n)); %conductive loss (MW)
    Qloss(n) = Qconv(n) + Qrad(n) + Qcond(n); %total losses


    if Qabs(n) == 0 && Tamb(n) == 273.15
    Qnet(n) = 0; % System off
    Qloss(n) = 0; % System Off
    else
     Qnet(n) = Qabs(n) - Qloss(n); % the net useful thermal power (MW) Qnet(n) = Qabs(n) - Qloss(n); % the net useful thermal power (MW)
    end

    end

end
```

Code 3 shows the computation of the energy per month before the Rankine cycle from the daily energy.

Code 3: Code for computing energy per month.

```
function Emonth = DailyEnergy(app, Qnet, DaysperMonth) % calculating the energy produced in per month.
    for n = 1:12
    Edaily(n) = Qnet(n)*3600*12;   % conversion from MW to MJ for 12 hour day generation
    Emonth(n) = Edaily(n)*DaysperMonth(n); % the total energy per month in MJ
    end
end
```

Code 4 shows the steps in converting the monthly energy into electricity by the Rankine cycle. The thermal energy loss per month was then computed, and lastly, the system efficiency was determined per month.

Code 4: Code for computing energy output, thermal energy loss and system efficiency.

```
function [EOutput, Eloss, etaSys] = ElecConversion(app, Emonth, Qloss, DaysperMonth, DNImonthly )%Calculate energy output in MWh,
    % energy losses in MWh and the syste efficiency
    etaRcycle = 0.43; % Rankine cycle efficiency
    Afield = 100000; % total heliostatic area m^2

    for n = 1:12
    Eelec(n) = Emonth(n)*etaRcycle; % Electrical Energy In MJ
    EOutput(n) = Eelec(n)/3600; % Energy in MWh

    Eloss(n) = Qloss(n)*12*DaysperMonth(n); %thermal energy loss in MWh

    if EOutput(n) == 0
    etaSys(n) = 0; %system off
    else
    etaSys(n) = (EOutput(n)/(12*DaysperMonth(n)))/(DNImonthly(n)*Afield)*100; % Determinning the monthly system efficiency
    end
    end
end
```

Code 5 shows the code in the computation of the thermal energy stored by the tank. It gives the capacity of the thermal battery in (MWh).

Code 5: Code for computing thermal energy stored in tank.

```
function EstorageMWh = energyStorage(app, Tr) %Energy storage Capacity of the TES system
    msalt = 18*(10^(6)); %Mass of the molten salt (kg) Solar Salt
    cpsalt = 1500; %specific heat capacity of salt [J/kg.K] Solar Salt
    Thot = Tr; %hot tank temperature (K)
    Tcold = 530; %cold tank temperature (K)

    for n = 1:12

    if Thot(n) == 273.15
    EstorageMWh(n) = 0; % System off
    elseif Thot(n) < 530 % Melting point of solar salt is 496
    EstorageMWh(n) = 0; % System off
    else
    EstorageJ(n) = msalt*cpsalt*(Thot(n)-Tcold); %Energy stored in Joules
    EstorageMWh(n) = EstorageJ(n)/(3600*(10^(6))); % Energy stored in MWh

    end

    end
end
```

References

Abaza, M.A., El-Maghlany, W.M., Hassab, M., & Abulfotuh, F. (2020). 10 MW concentrated solar power (CSP) plant operated by 100% solar energy: Sizing and techno-economic optimization. *Alexandria Engineering Journal*, *59*(1), 39-47. https://doi.org/10.1016/j.aej.2019.12.005

Abuashe, I., Shuia, E., & Aljermi, H. (2020). Modelling and simulation of concentrated solar power plant in Ber'Alganam area (Azzawia-Libya). *Solar Energy and Sustainable Development Journal*, *9*(2), 11-28. https://doi.org/10.51646/jsesd.v8i2.27

Agrafiotis, C., Pein, M., Eltayeb, A., Klaas, L., de Oliveira, L., Singh, A.K., & Sattler, C. (2023). Porous monolithic perovskite structures for high-temperature thermochemical heat storage in concentrated solar power (CSP) plants and renewable electrification of industrial processes. In *SolarPACES Conference Proceedings* (Vol. 2). TIB Open Publishing (Technische Informationbibliothek), Sydney, Australia. https://doi.org/10.52825/solarpaces.v2i.862

Alnaimat, F., & Rashid, Y. (2019). Advances in concentrated solar power: a perspective of heat transfer. In: Iranzo, A. (ed) *Heat and Mass Transfer-Advances in Science and Technology Applications* (pp. 1-17). Intech Open, London, United Kingdom. https://doi.org/10.5772/intechopen.84575

Atmaja, T.D., & Pikra, G. (2013). Absorber layer addition and thermal storage media comparison for concentrated solar power plant optimization. *Energy Procedia*, *32*, 74-83. https://doi.org/10.1016/j.egypro.2013.05.010

Bagré, B., Boukar, M., Muritala, I.K., Mortey, E.M., Ouarma, I., Tera, S., & Rabani, A. (2023). Modelling and simulation of a sustainable thermal energy storage system for concentrating solar power (CSP) plant using eco-materials. *JP Journal of Heat and Mass Transfer*, *31*, 147-161. http://dx.doi.org/10.17654/0973576323010

Bascom, A. (2025). Installation of solar PV systems, strategies and case studies–hybrid systems for Guyana. *Prabha Materials Science Letters*, *4*(2), 197-225. https://doi.org/10.33889/PMSL.2025.4.2.018

Bori, I., Jiya, J.Y., Orah, A.M., Bako, S., & Oyebamiji, M.O. (2024). Heat transfer analysis of a concentrated-type solar dryer for ginger. *Gazi University Journal of Science Part A: Engineering and Innovation*, *11*(4), 690-700. https://doi.org/10.54287/gujsa.1538840

Boribayeva, A., Gvozdeva, X., & Golman, B. (2024). Packing characteristics and heat transfer performance of non-spherical particles for concentrated solar power applications. *Energies*, *17*(18), 4552. https://doi.org/10.3390/en17184552

Catalano, A., Rocco, M., Toro, C., Colombo, E., & Sciubba, E. (2016). Simulation and comparative Thermoeconomic analysis of central receiver concentrated solar plants using air as heat transfer fluid. In *Proceedings of the 29th International Conference on Efficiency, Cost, Optimisation, Simulation and Environmental Impact of Energy Systems* (pp. 1-16). Portorož, Slovenia.

Cekirge, H.M., Erturan, S.E., & Thorsen, R.S. (2020a). CSP (concentrated solar power)—tower solar thermal desalination plant. *American Journal of Modern Energy*, *6*(2), 51-58. https://doi.org/10.11648/j.ajme.20200602.11

Cekirge, H.M., Erturan, S.E., & Thorsen, R.S. (2020b). The CSP (concentrated solar power) plant with Brayton cycle: a third generation CSP system. *American Journal of Modern Energy*, *6*(1), 43-50. https://doi.org/10.11648/j.ajme.20200601.16

Coco-Enríquez, L., Muñoz-Antón, J., & Martínez-Val, J.M. (2017). Dual Loop line-focusing solar power plants with supercritical Brayton power cycles. *International Journal of Hydrogen Energy*, *42*(28), 17664-17680. https://doi.org/10.1016/j.ijhydene.2016.12.128

Goortani, B.M., & Heidari, H. (2017). Advanced modeling of CSP plants with sensible heat storage: instantaneous effects of solar irradiance. *International Journal of Renewable Energy Research*, *7*(3), 1419-1425.

Grena, R., Lanchi, M., Frangella, M., Ferraro, V., Marinelli, V., & D'Auria, M. (2024). Thermal analysis of parabolic and Fresnel linear solar collectors using compressed gases as heat transfer fluid in CSP plants. *Energies*, *17*(16), 3880. https://doi.org/10.3390/en17163880

Hernández, B., Ferber, N.L., Abdullah, M., Mayyas, A., Calvet, N., & Chiesa, M. (2025). Central receiver-based concentrated solar power plants part 1: a historical review. *Solar Energy*, *299*, 113693. https://doi.org/10.1016/j.solener.2025.113693

Jawhar, N.S., Witharana, S., Nggada, S., Talib, A., Belachew, C., & Li, Y. (2020). Thermal energy storage options for concentrated solar power plants in the United Arab Emirates. In *2020 Advances in Science and Engineering Technology International Conference* (pp. 1-6). Institute of Electrical and Electronics Engineers, Dubai, United Arab Emirates. https://doi.org/10.1109/ASET48392.2020.9118241

Khan, M.I., Asfand, F., & Al-Ghamdi, S.G. (2022a). Progress in technology advancements for next generation concentrated solar power using solid particle receivers. *Sustainable Energy Technologies and Assessments*, *54*, 102813. https://doi.org/10.1016/j.seta.2022.102813

Khan, M.I., Asfand, F., & Al-Ghamdi, S.G. (2022b). Progress in research and development of phase change materials for thermal energy storage in concentrated solar power. *Applied Thermal Engineering*, *219*, 119546. https://doi.org/10.1016/j.applthermaleng.2022.119546

Kwasi-Effah, C.C., Ighodaro, O., Egware, H.O., & Obanor, A.I. (2024). Socioeconomic implications of a new quaternary molten salt heat transfer fluid for concentrated solar power plants. *NIPES-Journal of Science and Technology Research*, *6*(1), 70-74. https://doi.org/10.5281/zenodo.14043148

Nie, F., Bai, F., Wang, Z., Li, X., & Yang, R. (2022). Solid particle solar receivers in the next-generation concentrated solar power plant. *EcoMat*, *4*(5), e12207. https://doi.org/10.1002/eom2.12207

Onu, P., & Mbohwa, C. (2019). Concentrated solar power technology and thermal energy storage: a brief overview of nascent sustainable designs. In *2019 7th International Renewable and Sustainable Energy Conference* (pp. 1-4). IEEE. Agadir, Morocco.

Pan, X., Yuan, M., Ju, X., & Xu, C. (2023). A switchable concentrating photovoltaic/concentrating solar power (CPV/CSP) hybrid system for flexible electricity/thermal generation. *Science China Technological Sciences*, *66*(8), 2332-2345. https://doi.org/10.1007/s11431-023-2453-0

Pinello, L., Fossati, M., Giglio, M., Cadini, F., Bevilacqua, C., Cilento, M., Bassetti, F., & Magaldi, R. (2023). Structural performance-based design optimisation of a secondary mirror for a concentrated solar power (CSP) plant. *Energies*, *16*(16), 6000. https://doi.org/10.3390/en16166000

Reyes-Belmonte, M.A., Díaz, E., Romero, M., & González-Aguilar, J. (2018). Particles-based thermal energy storage systems for concentrated solar power. In *AIP Conference Proceedings* (Vol. 2033, No. 1, p. 210013). AIP Publishing LLC, Santiago, Chile. https://doi.org/10.1063/1.5067215

Shukir, S.S. (2022). Concentrated solar power (CSP) systems to solve the problem of the increasing in electricity demand in the summer season in Iraq. *Journal of Alternative and Renewable Energy Sources*, *8*(2), 9-15. https://doi.org/10.46610/JOARES.2022.v08i02.002

Starke, A.R., Lemos, L.F.L., Colle, S., Reinaldo, R.F., Cardemil, J.M., & Escobar, R. (2016). A methodology for simulation and assessment of concentrated solar power plants. *Revista De Engenharia Térmica, 15*(1), 33-40. https://doi.org/10.5380/reterm.v15i1.62162

Tahir, Z.R., Nisar, M.A., Ali, T., Mukhtar, M.F., Hassan, A., Awan, T.A., Mohsin, M.A., Asghar, F., Siddiqi, H.S., Azhar, M., Rasheed, W.H., Akhtar, T., & Asim, M. (2024). Performance assessment of 50 MWe concentrated solar power linear Fresnel reflector power plant in Pakistan. *Proceedings of the International Renewable Energy Storage and Systems Conference* (p. 224). Springer Nature, Aachen, Germany. https://doi.org/10.2991/978-94-6463-455-6_24

Toro, C., Rocco, M.V., & Colombo, E. (2016). Exergy and thermoeconomic analyses of central receiver concentrated solar plants using air as heat transfer fluid. *Energies*, *9*(11), 885. https://doi.org/10.3390/en9110885

Wang, G., Pang, S., & Jiang, T. (2023). A brief review of liquid heat transfer materials used in concentrated solar power systems and thermal energy storage devices of concentrated solar power systems. *Engineering Reports*, *5*(2), e12576. https://doi.org/10.1002/eng2.12576

Xu, B., Li, P., & Chan, C.L. (2015). Energy storage start-up strategies for concentrated solar power plants with a dual-media thermal storage system. *Journal of Solar Energy Engineering*, *137*(5), 051002. https://doi.org/10.1115/1.4030851

Yahya, A., Yessef, M., Lagrioui, A., Boutammachte, N., & Zhilenkov, A. (2024). Performance improvement and techno-economic optimization of Noor I solar power plant in Morocco using various heat transfer fluids. *IEEE Access*, *12*, 151204-151222. https://doi.org/10.1109/ACCESS.2024.3479970